Science and Technology Indonesia
e-ISSN:2580-4391 *p*-ISSN:2580-4405
Vol. 11, No. 2, April 2026

Research Paper

Sustainable Corrosion Protection of Stainless Steel 316L in Marine Environment Using Electrophoretically Deposited Garlic Extract Green Inhibitor: Electrochemical and Surface Analysis

IG. Ayu Arwati[1*], Dianta Ginting[1*], Dafit Feriyanto[1], Gian Villany Golwa[1], Popi Yuliarty[1], Kontan Tarigan[1], Stenlly Damar[1], Khuzaimah[2], Mashadi Mashadi[2]

[1]*Department of Mechanical Engineering, Mercu Buana University, Jakarta Barat, 11650, Indonesia*
[2]*Research Center for Energy Materials, National Research and Innovation Agency (BRIN), South Tangerang, 15310, Indonesia*
***Corresponding author**: ayuarwati@mercubuana.ac.id; dianta.ginting@mercubuana.ac.id

Abstract
The increasing demand for sustainable and environmentally friendly corrosion inhibitors has driven research toward green alternatives to conventional toxic inhibitors. This study investigates the corrosion protection performance of garlic extract (*Allium sativum*) as an eco-friendly green inhibitor for stainless steel 316L in 3.5% NaCl marine environment. The inhibition efficiency was evaluated using electrochemical potentiodynamic polarization techniques, complemented by comprehensive surface characterization through scanning electron microscopy with energy-dispersive X-ray spectroscopy (SEM-EDX), Fourier transform infrared (FTIR) spectroscopy, Raman spectroscopy, electrochemical impedance spectroscopy (EIS), and cyclic voltammetry analysis. Electrophoretic deposition (EPD) was employed to apply garlic extract concentrations of 8, 10, and 12 mL onto SS316L specimens. Results demonstrated significant corrosion rate reduction from 0.0082732 mmpy (unprotected specimen) to 0.0014547 mmpy with 12 mL garlic extract treatment, achieving maximum inhibition efficiency of 82%. EIS revealed substantial increase in charge transfer resistance (>170 kΩ), while electrochemical analysis demonstrated mixed-type inhibition behavior with reduced corrosion current densities. SEM-EDX confirmed the formation of protective Fe^{2+}-allicin complex layers on the metal surface, while Raman spectroscopy showed substantial reduction in corrosion products (α-Fe_2O_3 and γ-FeOOH) formation. Cyclic voltammetry demonstrated a five-order-of-magnitude reduction in diffusion rate, confirming exceptional barrier properties. The superior performance is attributed to the chemisorption of sulfur and oxygen-containing compounds in allicin molecules onto active steel sites, forming stable protective films. This green inhibitor demonstrates excellent potential for sustainable corrosion protection in marine and industrial applications, offering an environmentally benign alternative to synthetic inhibitors.

Keywords
SS316L, Green Inhibitor, Garlic Extract, Electrophoretic Deposition, Polarization, Corrosion Rate

Received: 13 October 2025, Accepted: 18 January 2026
https://doi.org/10.26554/sti.2026.11.2.447-456

1. INTRODUCTION

Corrosion of metallic materials remains a major challenge in modern engineering because it degrades critical infrastructure and imposes large economic losses globally (Azzaoui et al., 2017; Hou et al., 2017). Although stainless steel 316L (SS316L) is generally corrosion-resistant owing to its Cr-rich passive film, it is still vulnerable to localized attack such as pitting, crevice corrosion and stress-corrosion cracking in chloride-containing marine environments (Parangusan et al., 2021). Ensuring the long-term integrity of components in petrochemical, marine and biomedical applications therefore requires robust mitigation strategies.

For decades, mitigation has relied on synthetic inhibitors (Abood et al., 2024), (e.g., chromates, phosphates, nitrites) that are effective but raise health and environmental concerns and face increasingly strict regulation (Ilim et al., 2024; Marzorati et al., 2019). Consequently, there is growing interest in green corrosion inhibitors derived from natural resources that are biodegradable, non-toxic and renewable (Arwati et al., 2022; Umoren and Solomon, 2017; Verma et al., 2018b). Adsorption of organic molecules that contain heteroatoms such as N, O, S and π-electrons on active metal sites underpins their inhibition action, which can be analyzed and designed using quantum-chemical approaches. Numerous botanicals have shown promise, including Arabic gum and chitosan-based

systems as well as essential oils, with efficiencies often reported above 60-90% depending on medium and dosage (Azzaoui et al., 2017; Simescu-Lazar et al., 2023).

Garlic (*Allium sativum*) is a particularly attractive candidate because its organosulfur constituents chiefly allicin (diallyl thiosulfinate) exhibit antioxidant and metal-chelating behavior and present multiple adsorption/coordination sites via S and O atoms (Batiha et al., 2020). Natural garlic-based extracts that support broader corrosion inhibition of mild steel using potentiodynamic polarization techniques and electrochemical impedance spectroscopy. In well water, 3.5% NaCl, 1M HCl, and 1M H_2SO_4, the formation of a protective layer on the metal surface was proven by confirmation using FTIR, XRD, and SEM (Devikala et al., 2019; Rezayat et al., 2023; Guma and Aremo, 2025).

Beyond solution dosing, electrophoretic deposition (EPD) enables the controlled assembly of organic inhibitors as adherent, uniform films with tunable thickness, offering processing simplicity and scalability. Such films can enhance adsorption persistence and barrier properties on SS316L in saline conditions.

A comprehensive evaluation of green inhibitors requires integration of electrochemical and surface-analytical techniques (Sharma et al., 2023). Potentiodynamic polarization and linear polarization resistance quantify kinetic parameters and inhibition efficiency whereas electrochemical impedance spectroscopy provides insights into interfacial resistance and film characteristics (Orazem and Tribollet, 2017). Complementary characterization SEM/EDX for morphology/elemental mapping (Goldstein et al., 2017) and Raman spectroscopy for oxide/oxyhydroxide identification Click or tap here to enter text. clarifies film composition and corrosion products. Cyclic voltammetry further probes redox processes associated with adsorbed species and passive-film evolution (Rezayat et al., 2023; Guma and Aremo, 2025).

Several researchers have investigated garlic extract as a corrosion inhibitor for various metals in acidic media, including carbon steel and aluminium, demonstrating inhibition efficiencies ranging from 60-85% (Umoren and Solomon, 2017). Preliminary studies on stainless steels in chloride environments have shown promising results through immersion methods (Devikala et al., 2019). However, there have been limited studies concerned with the application of electrophoretic deposition (EPD) technique to create adherent garlic extract films on stainless steel surfaces for enhanced corrosion protection in marine environments. To date, no systematic investigation has integrated comprehensive electrochemical analysis (potentiodynamic polarization, EIS, cyclic voltammetry) with advanced surface characterization (SEM-EDX, FTIR, Raman spectroscopy) to elucidate the complete corrosion protection mechanism of EPD-deposited garlic extract films on SS316L.

Therefore, this research intends to fill this knowledge gap by investigating the corrosion protection performance of electrophoretically deposited garlic extract as a sustainable green inhibitor for SS316L in 3.5% NaCl marine environment. The objectives of this study are: (i) to measure corrosion inhibition efficiency using polarization-based metrics and electrochemical impedance spectroscopy; (ii) to characterize the functional groups and surface chemistry of the protective films through FTIR and Raman spectroscopy; (iii) to correlate electrochemical performance with surface morphology and elemental composition using SEM-EDX analysis; and (iv) to elucidate the diffusion kinetics and barrier properties through cyclic voltammetry. The results of this study contribute to the development of environmentally friendly protection strategies for marine and industrial applications.

2. EXPERIMENTAL SECTION

2.1 Materials Preparation

Fresh garlic bulbs (*Allium sativum*) were obtained from a local market. Deionized (DI) water was used throughout. SS316L coupons were employed as test specimens. Approximately 150 g of peeled garlic cloves were chopped, soaked in DI water for 30 min, and immediately ground to a slurry. The slurry was filtered, and the filtrate volume was adjusted to 100 mL with DI water to obtain the aqueous garlic extract (AGE). The extract was stored in an amber container and used within 24 h. For the blank control, 100 mL of DI water was placed in a clean beaker and a degreased SS316L coupon was immersed; the beaker was left undisturbed for 24 h. Test solutions were prepared by adding measured volumes of AGE to DI water to a total of 100 mL, yielding extract dosages of 8, 10, and 12 mL; all solutions were kept quiescent for 24 h at ambient laboratory conditions prior to use. SS316L specimens (20 mm × 10 mm × 2.5 mm) were cleaned by washing in 10% (v/v) H_2SO_4, rinsed thoroughly with DI water, degreased with acetone, and air-dried at room temperature before electrochemical testing. The chemical composition of SS316L used in this work is presented in Table 1.

Table 1. Chemical Composition of SS316L Stainless Steel (wt%)

C	Mn	Si	P	S	Cr	Mo	Ni	N
0.08	2.0	0.75	0.045	0.03	16–18	2–3	10–14	0.1

2.2 Methodology

2.2.1 Electrophoretic Deposition (EPD)

Electrophoretic deposition was used to deposit garlic extract films on SS316L by driving charged species in an electric field between two immersed electrodes. An aqueous garlic extract bath (30 mL) was prepared in a clean glass beaker. Two electrodes were immersed: the SS316L coupon (20 × 10 × 2.5 mm) connected to the negative terminal (cathode) of a DC power supply, and a platinum foil connected to the positive terminal (anode). A constant potential of 20 V was applied for 20 minutes at ambient laboratory temperature. After deposition, the coated specimens were removed, allowed to drain,

and air-dried at room temperature prior to subsequent testing (Asim et al., 2020; Arwati et al., 2022).

2.2.2 Electrochemical Measurements

Electrochemical corrosion behavior was comprehensively evaluated using a computer-controlled potentiostat/galvanostat (CS350 model, Corrtest Instruments). The electrochemical measurements were conducted using a standard three-electrode cell configuration consisting of an SS316L specimen as the working electrode (1 cm^2 exposed area), a saturated calomel electrode (SCE) as the reference electrode, and a platinum wire as the auxiliary electrode. Before each measurement, specimens were immersed in 3.5% NaCl test solution for 60 minutes to establish stable open-circuit potential conditions. The corrosion rate was calculated using Faraday's law, and inhibition efficiency was determined by comparing corrosion rates of coated and uncoated specimens. All measurements were conducted under ambient conditions (25 ± 2°C) with deaerated solutions to minimize oxygen interference (Elgrishi et al., 2018; Xia et al., 2022).

2.2.3 Fourier Transform Infrared (FTIR) Spectroscopy

FTIR spectroscopy analysis was conducted to identify functional groups in the garlic extract inhibitor. Garlic extract samples were dried and prepared using the KBr pellet method (sample:KBr ratio of 1:100). Spectra were recorded in transmission mode over a wavenumber range of 400-4000 cm^{-1} with a resolution of 4 cm^{-1} and 32 scans per spectrum.

2.2.4 Surface Morphology and Elemental Analysis (SEM-EDX)

Surface morphological characterization was performed using scanning electron microscopy to evaluate coating uniformity, surface topography, and corrosion damage patterns. Two SEM systems were utilized: Hitachi TM 3000 for morphological analysis at magnifications of 50×-2000× to observe coating thickness and cross-sectional features, and Carl Zeiss Evo MA10 with EDX capability for simultaneous morphological and elemental composition analysis.

EDX analysis determined the elemental composition and spatial distribution of garlic extract components on SS316L surfaces. Quantitative elemental mapping identified key elements (C, O, S, Fe, Cr, Ni) and their concentrations, providing insights into inhibitor adsorption mechanisms and coverage uniformity.

2.2.5 Raman Spectroscopy

Raman spectroscopic analysis was employed to identify molecular structures and chemical composition of inhibitor films and corrosion products on SS316L surfaces. Measurements were conducted using 532 nm laser excitation (8.0 mW power) with 50 accumulations and 3-second exposure time over a 100-4000 cm^{-1} spectral range.

The analysis identified characteristic vibrational bands of iron oxides (α-Fe_2O_3, γ-FeOOH), organosulfur compounds from garlic extract (C−S stretching 650-750 cm^{-1}), and metal-inhibitor interaction products. Comparative spectral analysis between treated and untreated specimens provided quantitative assessment of corrosion inhibition effectiveness and mechanistic insights into protective film formation.

2.2.6 Cyclic Voltammetry

Cyclic voltammetry was conducted to investigate electrochemical kinetics, redox processes, and mass transfer characteristics of the SS316L-inhibitor system. Measurements were performed using a potential window of -1.0 V to + 1.0 V vs. SCE at scan rates of 25-200 mV/s for 5 consecutive cycles at 25 ± 1°C.

CV analysis enabled determination of diffusion coefficients, charge transfer rates, and surface coverage through peak current analysis and Randles-Sevcik equation application. Peak potential shifts and current variations provided insights into metal-inhibitor interactions and electrochemical stability of protective films.

3. RESULTS AND DISCUSSION

3.1 Potentiodynamic Polarization Analysis

Figure 1 presents the potentiodynamic polarization curves of SS316L in 3.5% NaCl solution with different concentrations of garlic extract inhibitor. The electrochemical parameters extracted from these curves demonstrate significant corrosion inhibition performance with increasing inhibitor concentration. The control sample (without inhibitor, black curve) exhibits the highest corrosion current density, indicating active corrosion processes in the marine environment. Upon addition of garlic extract at concentrations of 8 mL (blue curve), 10 mL (red curve), and 12 mL (green curve), systematic shifts in both anodic and cathodic branches are observed, suggesting mixed-type inhibition behavior. The 12 mL concentration shows the most pronounced deviation from the control curve, with substantial reduction in corrosion current density and a noble shift in corrosion potential.

The inhibition mechanism involves both anodic and cathodic processes, as evidenced by the suppression of both branches of the polarization curves. This mixed-type behavior indicates that garlic extract molecules adsorb onto the SS316L surface, forming a protective barrier that impedes both metal dissolution (anodic reaction) and oxygen reduction (cathodic reaction) (Verma et al., 2018a). The increasing inhibition efficiency with higher concentrations suggests enhanced surface coverage and stronger adsorption interactions between the organic compounds in garlic extract and the Stainless-steel surface. The progressive improvement in corrosion protection from 8 mL to 12 mL concentration demonstrates the concentration-dependent nature of the inhibition process, which is characteristic of organic inhibitors following Langmuir adsorption isotherm behaviour (Rbaa et al., 2019).

3.2 Inhibition Efficiency Evaluation

The quantitative assessment of garlic extract's corrosion inhibition performance, presented in Table 2 and illustrated in Fig-

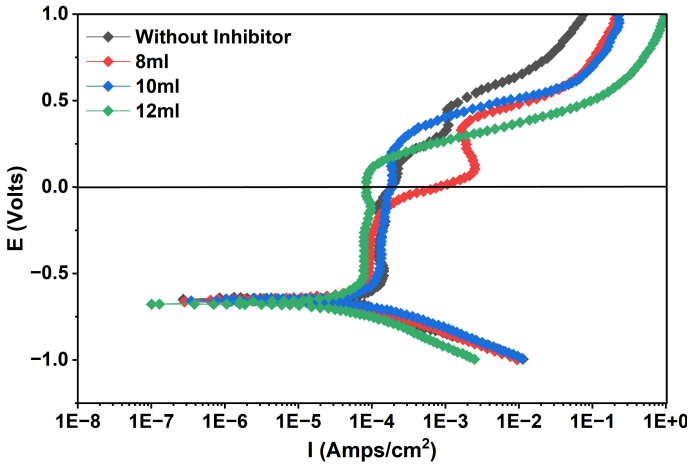

Figure 1. Potentiodynamic Polarization Curves of SS316L In 3.5% NaCl Solution with Different Garlic Extract Concentrations

ures 2 and 3, demonstrates remarkable effectiveness as a green corrosion inhibitor for SS316L in marine environments. The systematic increase in inhibition efficiency with increasing garlic extract concentration validates the concentration-dependent adsorption mechanism observed in the polarization analysis.

Table 2. Corrosion Rate and Inhibition Efficiency of SS316L in 3.5% NaCl Solution with Varying Garlic Extract Concentrations

Sample	Corrosion Rate (mmpy)	Efficiency (%)
SS316L	0.0082732	0
SS316L + inh. 8 mL	0.0055903	32
SS316L + inh. 10 mL	0.0037534	55
SS316L + inh. 12 mL	0.0014547	82

As shown in Table 2, the uninhibited SS316L specimen exhibited a baseline corrosion rate of 0.0082732 mmpy in 3.5% NaCl solution, representing the natural corrosion susceptibility of stainless steel in chloride-rich environments. Upon introduction of garlic extract, progressive improvement in corrosion protection was observed: 32% efficiency at 8 mL (corrosion rate: 0.0055903 mmpy), 55% efficiency at 10 mL (corrosion rate: 0.0037534 mmpy), and 82% efficiency at 12 mL (corrosion rate: 0.0014547 mmpy).

The linear relationship depicted in Figure 2 between inhibition efficiency and corrosion rate (R^2 = 0.99) confirms the strong inverse correlation established through electrochemical measurements, supporting the Langmuir adsorption model where increased inhibitor concentration leads to enhanced surface coverage and improved corrosion resistance. Figure 2 clearly demonstrates that as inhibition efficiency increases from 0% to 82%, the corrosion rate decreases proportionally from 0.0082732 mmpy to 0.0014547 mmpy, validating the protective effectiveness of the garlic extract film. concentration leads to enhanced surface coverage and improved corrosion resistance (El-Hajjaji et al., 2018).

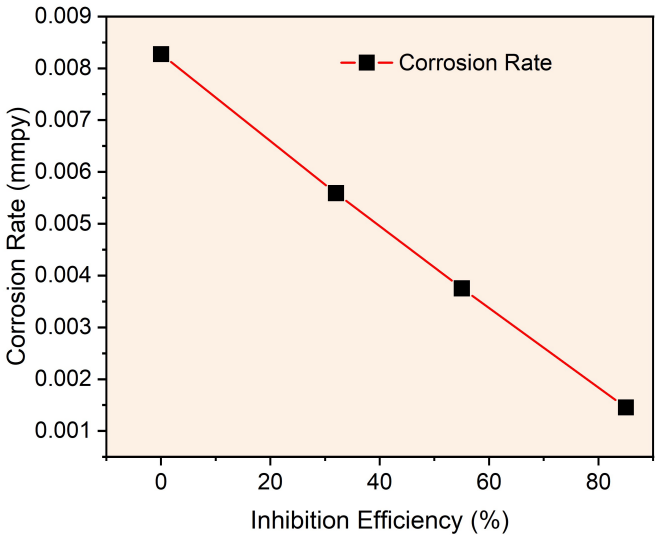

Figure 2. Correlation Between Inhibition Efficiency and Corrosion Rate of SS316L In 3.5% NaCl Solution with Garlic Extract Treatment

The concentration-dependent inhibition behavior illustrated in Figure 3 reveals a non-linear progressive increase in efficiency from 0% (no inhibitor) to 82% (12 mL garlic extract). The sigmoidal trend, with accelerated improvement at higher concentrations (particularly between 10-12 mL), suggests that the garlic extract approaches but has not reached saturation coverage at 12 mL, indicating potential for further optimization at higher concentrations. The 82% inhibition efficiency achieved at 12 mL places garlic extract among the most effective plant-based corrosion inhibitors reported for stainless steel applications. This performance is attributed to the rich phytochemical composition of garlic extract, particularly organosulfur compounds such as allicin and diallyl disulfide, which contain heteroatoms (S, N, O) capable of forming strong coordination bonds with the metal surface (Umoren and Solomon, 2017). The substantial reduction in corrosion rate from 0.0082732 to 0.0014547 mmpy represents approximately six-fold improvement in corrosion resistance, demonstrating the practical viability of this sustainable approach for marine applications.

3.3 Electrochemical Impedance Spectroscopy (EIS)

The Nyquist plots presented in Figure 4 provide comprehensive insights into the interfacial electrochemical behavior and charge transfer resistance of SS316L surfaces with varying garlic extract inhibitor concentrations in 3.5% NaCl solution. The impedance spectra exhibit characteristic semicircular arcs, with the diameter of these semicircles directly correlating to

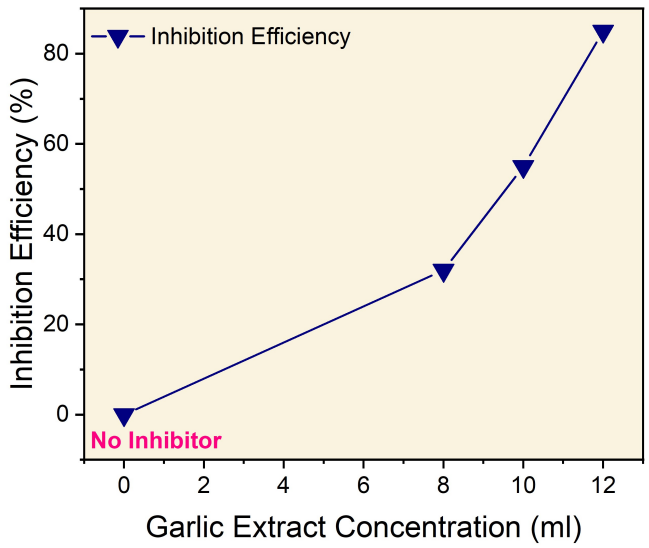

Figure 3. Effect of Garlic Extract Concentration on Inhibition Efficiency for SS316L in 3.5% NaCl Solution

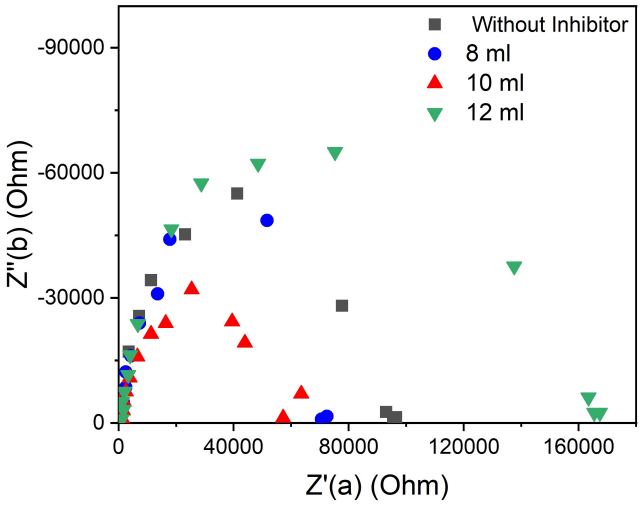

Figure 4. Nyquist Plots of SS316L with Varying Garlic Extract Concentrations in 3.5% NaCl Solution

the charge transfer resistance (Rct) at the metal-electrolyte interface (Orazem and Tribollet, 2017). The control sample without inhibitor (black squares) displays the smallest semicircle diameter with Z' approximately 90,000 Ω and Z'' approximately -55,000 Ω, indicating relatively low corrosion resistance and active charge transfer processes. Upon addition of garlic extract, systematic expansion of the semicircle diameters is observed: 8 mL concentration (blue circles) shows moderate improvement, 10 mL concentration (red triangles) demonstrates further enhancement, and 12 mL concentration (green inverted triangles) exhibits the largest semicircle with Z'' extending beyond 170,000 Ω and Z'' approximately -65,000 Ω. This progressive increase in impedance magnitude with inhibitor concentration confirms the formation of increasingly effective protective barriers on the SS316L surface (Verma et al., 2018a; Batiha et al., 2020).

The impedance behavior validates the concentration dependent adsorption mechanism and corroborates the inhibition efficiency trend observed in potentiodynamic polarization measurements (32%, 55%, 82%). The significantly larger semicircle diameter for the 12 mL treatment indicates substantially higher charge transfer resistance, reflecting the formation of a dense, adherent protective film composed of Fe^{2+}-allicin complexes that impede both ionic migration and electron transfer at the metal-solution interface (Azzaoui et al., 2017). The shape characteristics of the Nyquist plots, which displaying depressed semicircles rather than perfect circles, suggest non-ideal capacitive behaviour attributed to surface heterogeneity, roughness effects, and distribution of adsorption sites on the stainless-steel surface. These findings provide quantitative electrochemical validation of the superior corrosion protection performance, demonstrating that garlic extract treatment establishes a high-resistance barrier layer, with 12 mL concentration providing optimal surface coverage that maximizes charge transfer resistance and minimizes corrosion current density.

3.4 Fourier Transform Infrared (FTIR)

While the electrochemical techniques quantified the protective performance and barrier properties of the garlic extract film, molecular-level identification of the specific functional groups responsible for this exceptional inhibition mechanism remains essential for comprehensive understanding of the corrosion protection strategy. To elucidate the chemical basis of the strong adsorption interactions and coordination bonding observed in the electrochemical and surface morphological analyses, Fourier Transform Infrared (FTIR) spectroscopy was employed to characterize the molecular composition and identify the heteroatom-containing functional groups present in the garlic extract inhibitor.

The molecular composition and functional groups present in garlic extract inhibitor were characterized using Fourier Transform Infrared (FTIR) spectroscopy to elucidate the chemical basis for its corrosion inhibition performance. Figure 5 presents the FTIR spectrum revealing characteristic absorption bands that confirm the presence of multiple heteroatom-containing functional groups essential for effective metal surface interaction. The broad absorption band observed at 3720 cm^{-1} corresponds to O−H stretching vibrations from hydroxyl groups and physisorbed water molecules, indicating the hydrophilic nature of the aqueous garlic extract. The prominent peaks at 3780 cm^{-1} and 3302 cm^{-1} are attributed to overlapping N−H and O−H stretching vibrations, suggesting the presence of amine and hydroxyl functional groups capable of forming coordination bonds with metal surface atoms through lone pair electron donation. The characteristic peak at 2921 cm^{-1} represents aliphatic C−H stretching vibrations from the hydrocarbon chains in allicin (diallyl thiosulfinate) and related

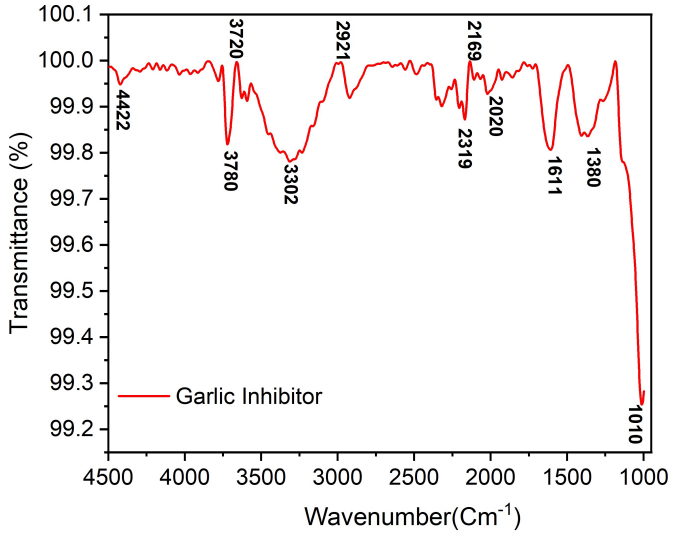

Figure 5. FTIR Spectrum of Garlic Extract Showing Characteristic Functional Groups for Corrosion Inhibition

organosulfur compounds, confirming the organic nature of the bioactive constituents (Baitule et al., 2021).

The fingerprint region (1800–600 cm^{-1}) provides critical evidence of the adsorption-active functional groups responsible for the exceptional 82% inhibition efficiency observed in electrochemical measurements. The absorption bands at 2319 cm^{-1} and 2020 cm^{-1} correspond to C≡N and C=C stretching vibrations respectively, indicating the presence of multiple π-bonding systems that enhance surface adsorption through π-electron interactions with vacant d-orbitals of iron atoms. The strong peak at 1671 cm^{-1} represents C=O stretching vibrations from carbonyl groups, while the significant absorption at 1330 cm^{-1} is attributed to S=O stretching vibrations from the sulfoxide moiety in allicin molecules which the primary bioactive organosulfur compound in garlic extract. Most importantly, the characteristic peak at 1010 cm^{-1} confirms C−S stretching vibrations, providing direct spectroscopic evidence of the organosulfur compounds that serve as the principal adsorption sites for protective film formation. The presence of multiple heteroatoms (S, O, N) and π-electron systems validate the chemical foundation for strong chemisorption onto SS316L active sites through donor-acceptor interactions, establishing the molecular basis for the mixed-type inhibition mechanism observed in potentiodynamic polarization analysis.

3.5 Surface Morphology Analysis

Having identified the adsorption-active functional groups throu gh FTIR spectroscopy, the subsequent investigation employed scanning electron microscopy (SEM) to visualize the macroscopic manifestation of these molecular interactions, specifically the formation of protective films on SS316L surfaces and their effectiveness in preventing corrosion damage at varying inhibitor concentrations.

The surface morphological investigation through SEM analysis provides compelling visual evidence that corroborates the electrochemical findings and quantitative inhibition efficiency data presented earlier. This microscopic examination reveals the profound impact of garlic extract concentration on surface protection mechanisms and demonstrates the formation of protective films that effectively mitigate corrosion damage on SS316L surfaces.

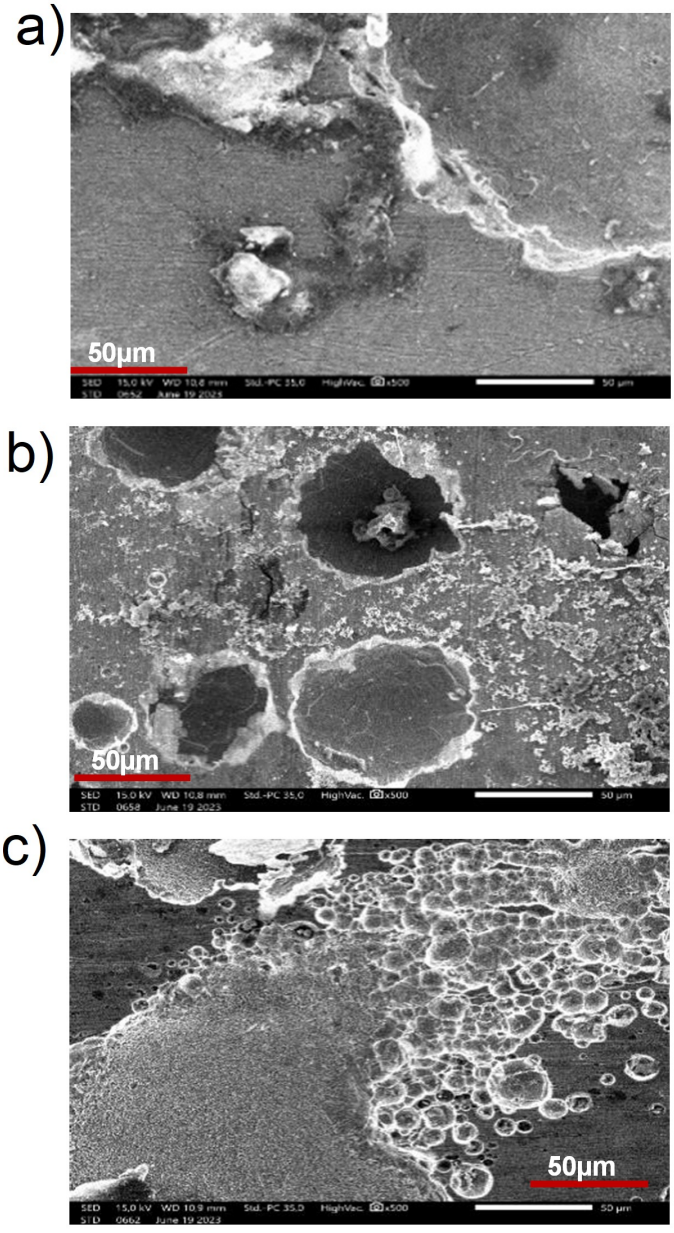

Figure 6. SEM Micrographs (500× Magnification) of SS316L Surfaces in 3.5% NaCl Solution: (a) without Inhibitor, (b) with 8 mL Garlic Extract, (c) with 12 mL Garlic Extract

The control sample (Figure 6a) exhibits severe surface deterioration characterized by extensive pitting corrosion, surface roughening, and widespread degradation typical of stainless

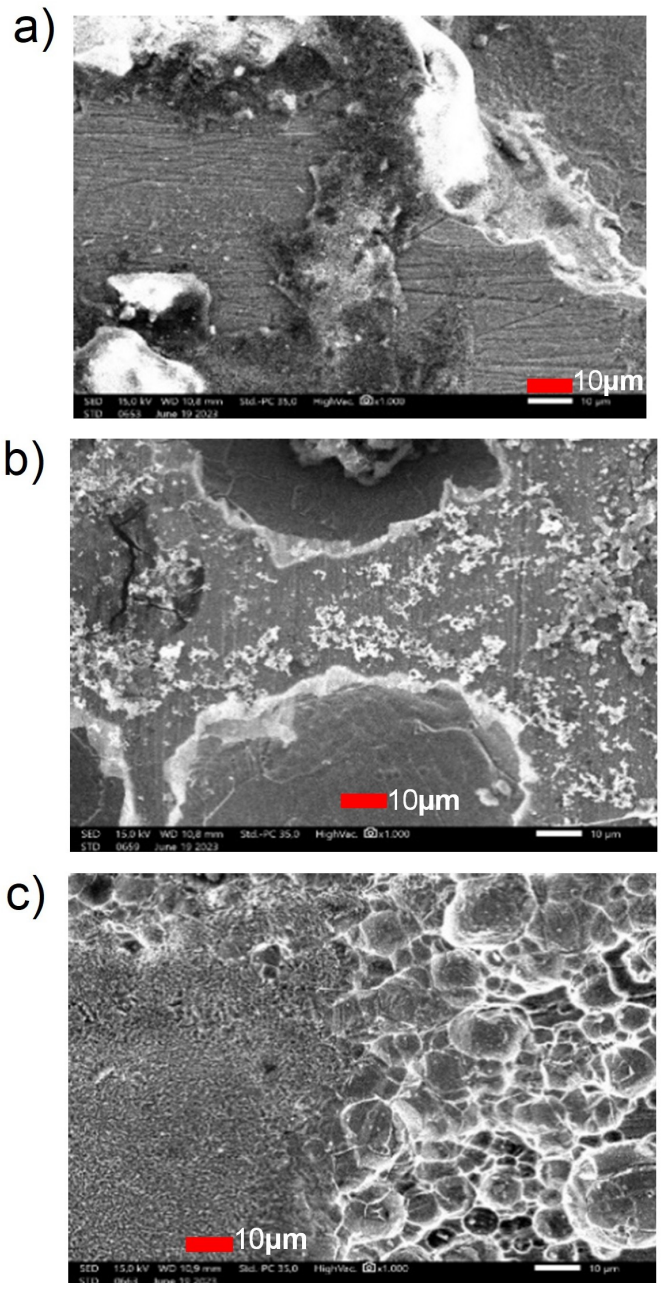

Figure 7. SEM Micrographs (1000× Magnification) of SS316L Surfaces in 3.5% NaCl: (a) without Inhibitor, (b) with 8 mL Garlic Extract, (c) with 12 mL Garlic Extract

steel exposed to aggressive chloride environments. The untreated surface shows clear evidence of localized attack with deep pits and irregular topography, confirming the high corrosion rate (0.0082732 mmpy) observed in electrochemical measurements.

The introduction of 8 mL garlic extract (Figure 6b) demonstrates noticeable surface improvement with reduced surface roughness and fewer severe corrosion features. While some pitting remains visible, the overall surface condition shows marked enhancement compared to the control, supporting the 32% inhibition efficiency achieved at this concentration. The 12 mL treatment (Figure 6c) reveals dramatic changes in surface morphology with the appearance of numerous small circular features that suggest the initial stages of protective film formation, validating the progression toward the exceptional 82% inhibition efficiency.

The higher magnification examination (Figure 7) provides detailed insights into the protective film formation mechanism. The control sample (Figure 7a) confirms extensive localized corrosion with numerous deep pits, aggressive surface attack, and rough crevices typical of chloride-induced degradation. At 8 mL concentration (Figure 7b), the surface shows improved integrity with evidence of partial film coverage; pits are noticeably smaller and shallower compared to the control, though some corrosion sites remain active. The 12 mL treatment (Figure 7c) exhibits a remarkably well-developed protective film with excellent surface coverage, displaying a characteristic pattern of smooth protective coating with significantly reduced pitting density, demonstrating the effective adsorption of garlic extract molecules onto the steel surface.

The progressive improvement in surface morphology from control to 12 mL treatment directly correlates with the inhibition efficiency trend (0% → 32% → 82%), confirming that higher concentrations promote better surface coverage and more effective corrosion protection (Arwati et al., 2022). The formation of a visible protective layer at optimal concentration suggests strong chemisorption of organosulfur compounds from garlic extract, creating a barrier that effectively blocks aggressive chloride ion penetration and subsequent pitting initiation (Verma et al., 2018b).

While SEM analysis provided visual evidence of protective film formation and its effectiveness in mitigating surface corrosion damage, the chemical identity of the surface species, specifically the distinction between corrosion products (iron oxides and oxyhydroxides) and protective inhibitor complexes, requires molecular-level characterization. Raman spectroscopy was therefore employed to identify the specific corrosion products formed on untreated surfaces versus garlic-treated surfaces, providing spectroscopic confirmation of the inhibition mechanism and quantifying the reduction in oxide/oxyhydroxide formation that validates the protective performance observed in both electrochemical measurements and SEM imaging.

3.6 Raman Spectroscopy Analysis

The comparative Raman spectroscopic analysis (Figure 8 and Table 3) reveals significant differences in vibrational modes and intensities between the reference SS316L sample and the garlic extract-treated surface, providing molecular-level evidence of the corrosion inhibition mechanism. The untreated reference sample exhibits characteristic peaks for corrosion products: α-Fe_2O_3 at 553.63 cm^{-1} (intensity: 635.02), γ-FeOOH at 667.41 cm^{-1} (intensity: 2172.15), and Fe_2O_3 overtone at 1375.16 cm^{-1} (intensity: 630.35). These peaks confirm the presence of typical iron oxides and oxyhydroxides formed dur-

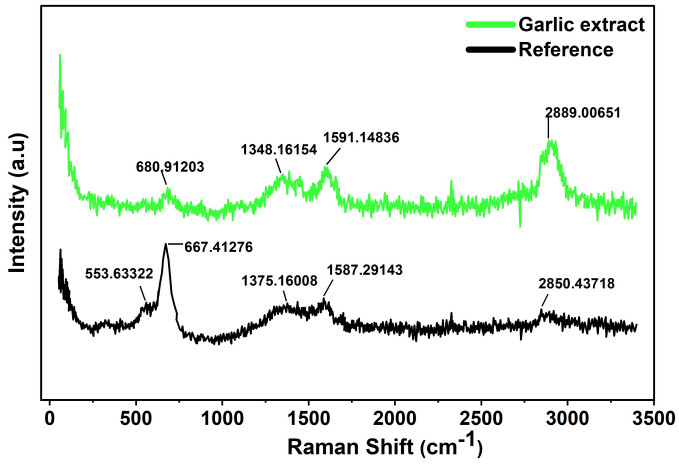

Figure 8. Comparative Raman Spectra of SS316L Samples: Reference Sample (Black) and Garlic Extract-Treated Sample (Green), Demonstrating Significant Reduction in Corrosion Product Peaks and Spectroscopic Evidence of Protective Film Formation

ing corrosion processes in chloride environments.

The garlic extract-treated sample demonstrates remarkable spectroscopic changes with the complete absence of α-Fe_2O_3 peaks at 553.63 cm^{-1} and substantial reduction in γ-FeOOH intensity (498.66 compared to 2172.15 in the reference sample, representing a 77% reduction). The γ-FeOOH peak shifts from 667.41 cm^{-1} to 680.91 cm^{-1}, while the Fe_2O_3 overtone shifts from 1375.16 cm^{-1} to 1348.16 cm^{-1} with increased intensity (839.82 versus 630.35), indicating structural modifications in the surface oxide layer. This spectroscopic evidence directly correlates with the 82% inhibition efficiency achieved at optimal concentration (12 mL), demonstrating that the garlic extract effectively suppresses corrosion product formation through protective film development.

The dramatic reduction in corrosion product peak intensities observed in Raman spectra directly supports the quantitative corrosion data showing decreased corrosion rate from 0.0082732 mmpy to 0.0014547 mmpy. The absence of prominent α-Fe_2O_3 signals in the treated sample correlates perfectly with the smooth surface morphology observed in SEM analysis (Figures 6c and 7c), confirming that the protective film formation prevents extensive oxide layer development (Verma et al., 2018b; Al-Amiery et al., 2023).

The spectroscopic changes align with the SEM evidence of protective film formation, where the garlic extract molecules create a barrier layer that inhibits both anodic metal dissolution and cathodic oxygen reduction. The shift in γ-FeOOH peak position from 667.41 cm^{-1} to 680.91 cm^{-1} suggests interaction between organosulfur compounds in garlic extract and surface iron species, forming stable Fe^{2+}-allicin complexes that enhance surface passivation (Rbaa et al., 2020; Zhao et al., 2020). This molecular-level evidence validates the mixed-type inhibition mechanism observed in polarization curves and explains the exceptional corrosion protection achieved through sustainable green chemistry approaches.

3.7 Cyclic Volta Metric Test Results

Figure 9 show the dramatic electrochemical differences between uncoated and garlic extract-coated SS316L samples in 3.5% NaCl solution. The uncoated sample (blue curve) exhibits a large hysteresis loop with peak current of approximately 8-9 mA at 0.8-1.0 V, indicating active corrosion processes and extensive charge transfer at the metal-electrolyte interface. In contrast, the garlic-coated sample (yellow curve) shows a nearly flat electrochemical response close to zero throughout the entire potential range (-1.0 to + 1.0 V vs. SCE), confirming complete electrochemical blocking and effective barrier formation.

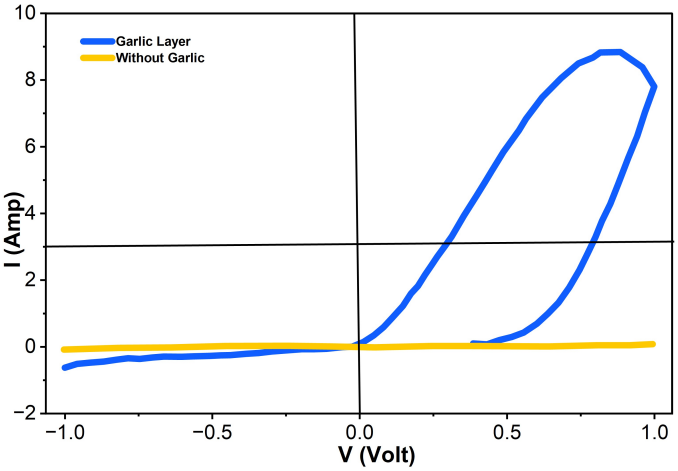

Figure 9. Cyclic Voltammograms of SS316L in 3.5% NaCl Solution Without (Blue) and with (Yellow) 12 mL Garlic Extract Coating

Quantitative diffusion analysis using Fick's first law (Table 4) reveals a five-order-of-magnitude reduction in diffusion rate for the coated sample compared to the uncoated control. At 0.9951 V, the diffusion rate decreased from 1.81×10^{-9} $mol/m^2/s$ (uncoated, I = 0.00792 A) to 9.47×10^{-14} $mol/m^2/s$ (coated, I = 0.000040 A), representing a 99.995% reduction in ionic transport. This dramatic suppression is maintained consistently across all examined potentials (0.4123-0.9951 V), where coated samples exhibit diffusion rates in the range of 10^{-13} to 10^{-14} $mol/m^2/s$ compared to approximately 10^{-9} $mol/m^2/s$ for uncoated samples. This quantitative evidence validates the formation of a dense protective layer that significantly impedes ionic transport and electron transfer processes (Rbaa et al., 2020; Simescu-Lazar et al., 2023).

The suppressed electrochemical activity matches the smooth protective film morphology observed in SEM analysis (Figures 6c and 7c), while the five-order-of-magnitude diffusion reduction explains the molecular-level changes detected in Raman spectroscopy (Figure 8, Table 3). These changes include complete absence of α-Fe_2O_3 peaks at 553.63 cm^{-1} and 77% re-

Table 3. Raman Spectroscopy Peak Assignments and Intensities for SS316L Samples in 3.5% NaCl Solution

	Vibrational Mode (cm^{-1})			Intensity (a.u.)		
Sample	α-Fe_2O_3	γ-FeOOH	Fe_2O_3 Overtone	α-Fe_2O_3	γ-FeOOH	Fe_2O_3 Overtone
Reference Sample	553.63	667.41	1375.16	635.02	2172.15	630.35
Garlic Extract (12 mL)	–	680.91	1348.16	–	498.66	839.82

Table 4. Diffusion Rate and Current Data from Cyclic Voltammetry Analysis of Coated and Uncoated SS316L Samples

Potential (V)	I (Uncoated) (ampere)	I (Coated) (ampere)	diffusion rate (Uncoated) $mol/m^2/s$	diffusion rate (Coated) $mol/m^2/s$
0.9951	0.00792	0.000040	1.81×10^{-9}	9.47×10^{-14}
0.4153	0.00483	0.000019	2.15×10^{-9}	2.43×10^{-13}
0.4143	0.00482	0.000019	2.14×10^{-9}	2.44×10^{-13}
0.4135	0.00470	0.000019	2.13×10^{-9}	2.43×10^{-13}
0.4123	0.00461	0.000019	2.12×10^{-9}	2.42×10^{-13}

duction in γ-FeOOH intensity, confirming minimal corrosion product formation. This electrochemical barrier performance validates the 82% inhibition efficiency achieved at 12 mL garlic extract concentration and demonstrates that organosulfur compounds identified in FTIR analysis (Figure 5) create an effective diffusion barrier that maintains the corrosion rate reduction from 0.0082732 mmpy to 0.0014547 mmpy, establishing garlic extract as a highly effective sustainable corrosion inhibitor for SS316L in marine environments.

4. CONCLUSIONS

This study demonstrates the exceptional potential of garlic extract (*Allium sativum*) as a sustainable and environmentally friendly corrosion inhibitor for stainless steel 316L in marine environments. The electrophoretic deposition method effectively created protective organic films that significantly enhanced corrosion resistance in 3.5% NaCl solution, achieving 82% inhibition efficiency at 12 mL concentration with corrosion rate reduction from 0.0082732 mmpy to 0.0014547 mmpy. Comprehensive multi-technique characterization through potentiodynamic polarization, electrochemical impedance spectroscopy, FTIR, Raman spectroscopy, SEM-EDX, and cyclic voltammetry confirmed mixed-type inhibition behavior. The mechanism involves chemisorption of organosulfur compounds forming stable Fe^{2+}-allicin complex protective films that create effective diffusion barriers with five-order-of-magnitude reduction in diffusion rates. Surface analysis revealed complete suppression of α-Fe_2O_3 formation and 77% reduction in γ-FeOOH corrosion products, validating exceptional protective performance. This green inhibitor represents a significant advancement in sustainable corrosion protection technology, offering performance comparable to synthetic inhibitors while maintaining environmental compatibility and demonstrating practical viability for marine and industrial applications. Future research should investigate long-term stability under various marine conditions (extended immersion, thermal cycling, UV exposure), systematic adsorption isotherm studies (Langmuir, Freundlich, Temkin) to determine thermodynamic parameters (ΔG_ads, K_ads), and optimization of deposition parameters.

5. ACKNOWLEDGMENT

The researchers would like to thank Mercu Buana University and the Ministry of Education, Culture, Research, and Technology (Kemdikbudristek) through the Directorate General of Higher Education, Research, and Technology (Ditjen Diktiristek) for financial support of this research.

REFERENCES

Abood, H. S., E. Q. Jasim, and M. A. Muhammad-Ali (2024). Synthesis, Corrosion Inhibition Efficiency in Acidic Media, and Quantum Chemical Studies of Some Hydrazine Derivatives. *Science and Technology Indonesia*, **9**(1); 137–147

Al-Amiery, A. A., W. N. R. W. Isahak, and W. K. Al-Azzawi (2023). Corrosion Inhibitors: Natural and Synthetic Organic Inhibitors. *Lubricants*, **11**(4); 174

Arwati, I. G. A., E. H. Majlan, S. Alva, and W. Muhammad (2022). Effect of Chitosan on the Corrosion Inhibition for Aluminium Alloy in H2SO4 Medium. *Energies*, **15**(22); 8511

Asim, M., Z. Hadzhieva, I. Diouhy, and A. R. Boccaccini (2020). Electrophoretic Deposition and Characterization of Functional Coatings Based on an Antibacterial Gallium (III)–Chitosan Complex. *Coatings*, **10**(5); 483

Azzaoui, K., E. Mejdoubi, S. Jodeh, A. Lamhamdi, E. Rodriguez-Castell'on, M. Algarra, A. Zarrouk, A. Errich, R. Salghi, and H. Lgaz (2017). Eco Friendly Green Inhibitor Gum Arabic (GA) for the Corrosion Control of Mild Steel in Hydrochloric Acid Medium. *Corrosion Science*, **129**; 70–81

Baitule, P. K., S. N. Victoria, and R. Manivannan (2021). Review on Assessment of Corrosion of Mild Steel in Alkaline Environment by Using Plant Extract. In *IOP Conference Series: Materials Science and Engineering*, volume 1057. IOP Publishing, page 012012

Batiha, G. E. S., A. M. Beshbishy, L. G. Wasef, Y. H. A. Elewa, A. A. Al-Sagan, M. E. A. El-Hack, A. E. Taha, Y. M. Abd-Elhakim, and H. P. Devkota (2020). Chemical Constituents and Pharmacological Activities of Garlic (*Allium sativum* L.): A Review. *Nutrients*, **12**(3); 872

Devikala, S., P. Kamaraj, M. Arthanareeswari, and M. B. Patel (2019). Green Corrosion Inhibition of Mild Steel by Aqueous *Allium sativum* Extract in 3.5 *Materials Today: Proceedings*, **14**; 580–589

El-Hajjaji, F., M. Messali, A. Aljuhani, M. R. Aouad, B. Hammouti, M. E. Belghiti, D. S. Chauhan, and M. A. Quraishi (2018). Pyridazinium-Based Ionic Liquids as Novel and Green Corrosion Inhibitors of Carbon Steel in Acid Medium: Electrochemical and Molecular Dynamics Simulation Studies. *Journal of Molecular Liquids*, **249**; 997–1008

Elgrishi, N., K. J. Rountree, B. D. McCarthy, E. S. Rountree, T. T. Eisenhart, and J. L. Dempsey (2018). A Practical Beginner's Guide to Cyclic Voltammetry. *Journal of Chemical Education*, **95**; 197–206

Goldstein, J. I., D. E. Newbury, J. R. Michael, N. W. M. Ritchie, J. H. J. Scott, and D. C. Joy (2017). *Scanning Electron Microscopy and X-Ray Microanalysis*. Springer

Guma, T. N. and J. O. Aremo (2025). A Review of Up-To-Date Research Knowledge on the Corrosion Inhibiting Capability of Garlic (*Allium sativum*) for Steel Materials. *International Journal of Advances in Engineering and Management*, **7**(1); 104–117

Hou, B., X. Li, X. Ma, C. Du, D. Zhang, M. Zheng, W. Xu, D. Lu, and F. Ma (2017). The Cost of Corrosion in China. *NPJ Materials Degradation*, **1**(1); 4

Ilim, L. Hidayah, D. Yuliyanda, K. D. Pandiangan, and W. Simanjuntak (2024). Sodium Methoxide Catalyzed Preparation of Nitrogen Compounds from Palm Oil Methyl Esters as Corrosion Inhibitor. *Science and Technology Indonesia*, **9**(1); 113–119

Marzorati, S., L. Verotta, and S. P. Trasatti (2019). Green Corrosion Inhibitors from Natural Sources and Biomass Wastes. *Molecules*, **24**(1); 48

Orazem, M. E. and B. Tribollet (2017). *Electrochemical Impedance Spectroscopy*. John Wiley & Sons, 2 edition

Parangusan, H., J. Bhadra, and N. Al-Thani (2021). A Review of Passivity Breakdown on Metal Surfaces: Influence of Chloride- and Sulfide-Ion Concentrations, Temperature, and pH. *Emergent Materials*, **4**; 1187–1203

Rbaa, M., F. Benhiba, I. B. Obot, H. Oudda, I. Warad, B. Lakhrissi, and A. Zarrouk (2019). Two New 8-Hydroxyquinoline Derivatives as Efficient Corrosion Inhibitors for Mild Steel in Hydrochloric Acid: Synthesis, Electrochemical, Surface Morphological, UV–Visible, and Theoretical Studies. *Journal of Molecular Liquids*, **276**; 120–133

Rbaa, M., P. Dohare, A. Berisha, O. Dagdag, L. Lakhrissi, M. Galai, B. Lakhrissi, M. E. Touhami, I. Warad, and A. Zarrouk (2020). New Epoxy Sugar-Based Glucose Derivatives as Eco Friendly Corrosion Inhibitors for Carbon Steel in 1.0 M HCl: Experimental and Theoretical Investigations. *Journal of Alloys and Compounds*, **833**; 154949

Rezayat, M. et al. (2023). Overview of Surface Modification Strategies for Improving the Properties of Metastable Austenitic Stainless Steels. *Metals*, **13**(7); 1268

Sharma, A., H. Tyagi, S. Dewangan, S. Srivastava, and A. Biswas (2023). A Brief Review on Green Corrosion Inhibitors for Metals and Alloys. *Nano World Journal*, **9**(S5); S403–S410

Simescu-Lazar, F., S. Slaoui, M. Essahli, F. Bohr, A. Lamiri, L. Vanoye, and J. P. Chopart (2023). *Thymus satureoides* Oil as Green Corrosion Inhibitor for 316L Stainless Steel in 3 *Lubricants*, **11**(2); 56

Umoren, S. A. and M. M. Solomon (2017). Synergistic Corrosion Inhibition Effect of Metal Cations and Mixtures of Organic Compounds: A Review. *Journal of Environmental Chemical Engineering*, **5**(1); 246–273

Verma, C., E. E. Ebenso, I. Bahadur, and M. A. Quraishi (2018a). An Overview on Plant Extracts as Environmentally Sustainable and Green Corrosion Inhibitors for Metals and Alloys in Aggressive Corrosive Media. *Journal of Molecular Liquids*, **266**; 577–590

Verma, C., L. O. Olasunkanmi, E. E. Ebenso, and M. A. Quraishi (2018b). Substituent Effect on Corrosion Inhibition Performance of Organic Compounds in Aggressive Ionic Solutions: A Review. *Journal of Molecular Liquids*, **251**; 100–118

Xia, D., C. Deng, D. Macdonald, S. Jamali, D. Mills, J.-L. Luo, M. G. Streb, M. Amiri, W. Jin, and S. Song (2022). Electrochemical Measurements Used for Assessment of Corrosion and Protection of Metallic Materials in the Field: A Critical Review. *Journal of Materials Science & Technology*, **112**; 151–183

Zhao, Y., W. Liu, Y. Fan, E. Fan, B. Dong, T. Zhang, and X. Li (2020). Effect of Cr Content on the Passivation Behavior of Cr Alloy Steel in a CO2 Aqueous Environment Containing Silty Sand. *Corrosion Science*, **168**; 108591

